Transactions of Tianjin University (2020) 26:135–141
https://doi.org/10.1007/s12209-020-00238-8

RESEARCH ARTICLE

Enhancing the Stability of Passive Film on 304 SS by Chemical Modification in Alkaline Phosphate–Molybdate Solutions

Chengcheng Pan[1,2] · Yang Song[1,2] · Weixian Jin[3] · Zhenbo Qin[1,2] · Shizhe Song[1,2] · Wenbin Hu[1,2] · Da-Hai Xia[1,2]

Received: 17 January 2020 / Revised: 1 February 2020 / Accepted: 5 February 2020 / Published online: 19 February 2020

Abstract

The purpose of this work was to enhance the corrosion resistance of the passive film on 304 stainless steel (SS) by chemical modification in alkaline phosphate–molybdate solutions. The 304 SS was passivated in both phosphate and phosphate–molybdate mixed solutions to investigate the effect of molybdate on its corrosion resistance. The experimental results indicated that the passive film showed better corrosion resistance in Cl^--containing solutions after modification in phosphate–molybdate solutions than in phosphate-only solutions. Energy-dispersive spectroscopy analyses revealed that the passive film formed in phosphate–molybdate solutions contained Mo and P after modification, which is the reason for the enhanced corrosion resistance.

Keywords Passive film · 304 SS · Corrosion · Phosphate · Molybdate

Introduction

304 stainless steel (SS) is extensively used as an engineering material due to its superior corrosion resistance, good appearance, and mechanical properties [1]. The passive film formed on 304 SS, with a thickness of several nanometers, plays a major role in protecting it from corrosion [2, 3]. However, 304 SS cannot be used for extended periods of time in marine environments, which are rich in Cl^- [4]. Cl^- can adsorb onto the surface of the passive film and may penetrate into the film and reach the film/substrate interface, thereby causing stress at the interface and film breakdown [5]. The mechanism of passive film breakdown induced by Cl^- is still a matter of debate [6–9], but is believed to be highly dependent on the nature of the materials [10–13]. Regardless of the specific mechanism of passivity breakdown, it is of great importance to develop surface modification methods to inhibit Cl^- attack.

Various methods have been developed to enhance the stability of this passive film, including chemical modification [14, 15], electroless plating [16, 17], electroplating [18], diffusion and infiltration technology [19], laser surface modification [20], and ion implantation [21]. Of these, the chemical modification method is favored for its flexibility and minimal consumption of electrical energy. The composition, thickness, and structure of a passive film can be modified by adjusting the chemical conditions of the solution, such as the pH and concentration of inorganic ions. Mo- or P-containing passive films are beneficial to passivity, leading to an increased corrosion potential [22–24]. Phosphate and molybdate have been considered to be beneficial passivators for carbon steel, aluminum alloy, and zinc [25, 26]. However, passivation in molybdate-only solution has resulted in a film with cracks [27]. Phosphate and molybdate have been reported to possibly have a synergistic effect on the passivation process, leading to the formation of a surface film with superior corrosion resistance [28, 29].

Here, we describe our surface modification experiments in alkaline phosphate–molybdate solutions. The corrosion resistances of the resulting passive films were evaluated by electrochemical impedance spectroscopy (EIS), and their compositions were determined by energy-dispersive spectroscopy (EDS).

✉ Da-Hai Xia
dahaixia@tju.edu.cn

1 Tianjin Key Laboratory of Composite and Functional Materials, Tianjin 300354, China

2 School of Materials Science and Engineering, Tianjin University, Tianjin 300354, China

3 Zhoushan Marine Corrosion Institute of Central Research Institute of Iron and Steel, Zhoushan 316003, China

Experimental

Material

The 304 SS, which was provided by Taiyuan Iron and Steel Co., was cut into plates with a dimension of 10 mm × 10 mm × 2 mm. They were then welded to a copper wire and embedded in epoxy resin, exposing a surface with 1 cm^2 in area. The prepared samples were abraded with 2000-grit SiC paper, cleaned with distilled water, acetone, and ethanol, and then dried with a hair drier.

Acid Picking

Prior to the passivation tests, we removed the surface oxide layer by immersing the specimens in a solution containing HNO_3 (4%) and HCI (36%) at 40 °C for 5 min and then washing them in a solution containing HNO_3 (7%), H_2SO_4 (9%), and HF (5%), at 25 °C for 1 min (concentration listed in mass fractions). All the solutions were exposed to air.

Passivation of 304 SS

After acid picking, the specimens were immediately placed in the passivation solutions. In this work, two solutions were used to modify the composition of the passive film formed on the 304 SS, as shown in Table 1. Solution A included NaOH, $NaNO_2$, and $NaPO_3$. Na_2MoO_4 (1%) was added to solution B to investigate the effect of molybdate on the corrosion resistance of the passive film. For comparison, a blank sample was used that had not been subjected to acid picking or passivation processing. Both solutions were exposed to air, and the passivation time lasted for 20–40 min. After the passivation process, the specimens were taken out, cleaned with distilled water, and blow-dried with a hair drier.

Electrochemical Impedance Spectroscopy

EIS measurement was taken at a VersaSTAT 3 electrochemical workstation (Princeton Applied Research, USA). To obtain a stable corrosion potential, after chemical passivation, we immersed the prepared specimen in a 3.5% (mass fraction) NaCl solution for about 20 min. The frequency used in the EIS measurement was set to range from 100 kHz to 10 mHz, with a peak-to-peak amplitude of the potential sinusoidal wave of 20 mV. With nine points for each frequency decade, the total number of data points was 63. The EIS data were fitted using ZSimpWin software.

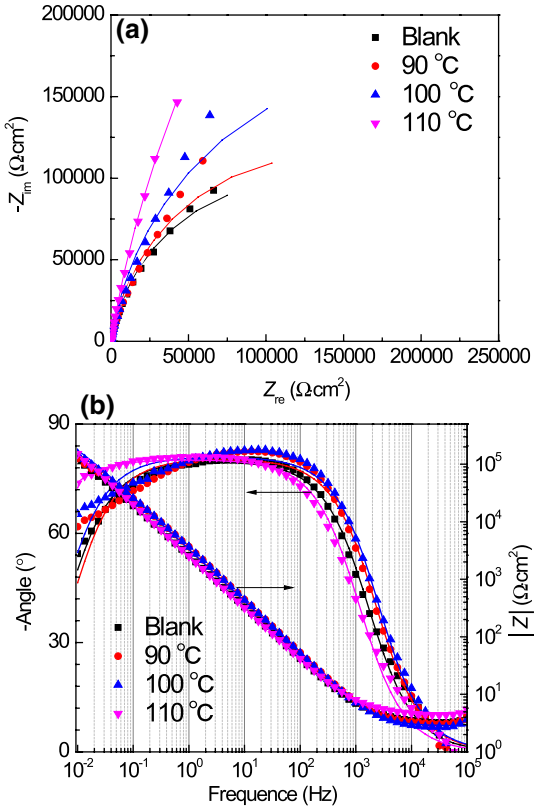

Fig. 1 Electrochemical impedance spectra of passivated 304 SS in 3.5% NaCl solution. **a** Nyquist plots, **b** Bode plots

Scanning Electron Microscopy (SEM) and EDS

SEM and EDS were performed using a Su1510 SEM (Hitachi, Japan) equipped with a model 550i energy-dispersive spectrometer.

Results

Passivation Behavior in Alkaline Phosphate Solution

Figure 1 shows the EIS measurements for the 304 SS after passivation in solution A at various temperatures (90 °C,

Table 1 Composition of passivation solution and other conditions

Solution	NaOH (wt%)	$NaNO_2$ (wt%)	Na_3PO_4 (wt%)	Na_2MoO_4 (wt%)	Temperature (°C)	Immersion time (min)
A	14	0.2	3	0	90–110	20–40
B	14	0.2	3	1	40–110	30

100 °C, and 110 °C). All the original data are depicted as points, and the corresponding fitting results are shown as lines. For passive metal covered by a layer of oxide film, an electrochemical equivalent circuit (EEC) of R_s (QR_t) can be used to simulate the electrochemical interface [30, 31], where R_s is the solution resistance, Q is the interface capacitance and is the constant phase element (CPE) related to the capacitance of the barrier layer (n is the dispersion coefficient for the CPE), and R_t is the charge transfer resistance, which is equal to the polarization resistance. We note that the most suitable EEC remains a matter of debate. For instance, Hien et al. [32] and Nam et al. [33] used an EEC that has two time constants. However, fitting the EIS data using their EEC generated huge errors in this work; therefore, we used a simple EEC that has been extensively used and reported in Refs. [30, 31].

Table 2 lists all the fitting results, including the fitting errors. All the Nyquist plots shown in Fig. 1a are characterized by an incomplete capacitance arc due to the very high polarization resistance of the electrochemical system. The diameter of the capacitance arc is approximately equal to R_t, and it can be seen that the diameter increases as the temperature increases from 90 to 110 °C. In this work, we did not use temperatures higher than 110 °C because a glass electrolytic cell works well only at temperatures less than 110 °C. The Bode plots in Fig. 1b indicate that as the temperature continues to increase, the impedance module values increase and the value of phase angle also increases. All the values of phase angle are negative because the imaginary part of the impedance is negative. The interface capacitance does not vary to a great extent, possibly because the number of adsorbed anions on the film surface alters just slightly. Nahali et al. [34] claimed that PO_4^{3-} can interact with Fe^{3+} and Fe^{2+} to form non-soluble $FePO_4$ and $Fe_3(PO_4)_2$, respectively, which is beneficial to the passivation process. Table 2 shows that as the temperature elevates, R_t increases accordingly and reaches 1.365×10^6 Ω cm^2 at 110 °C, which is ~6 times higher than that of the blank sample. The reason that a high temperature is beneficial for the corrosion resistance of the passive film is possibly due to the increase in the film thickness at high temperature [35].

In the last section, we describe our determination of the optimal condition and further investigate the impact of passivation time on the corrosion resistance of 304 SS. Figure 2 shows the measured EIS data for various passivation times, and Table 3 lists the fitting results obtained using the EEC shown in Fig. 3. As shown in Fig. 2a, the diameter of the capacitance arc increases as the passivation time is prolonged from 20 to 30 min. Further increasing the passivation time from 30 to 40 min has little impact on film resistance. The Bode plots show trends similar to those of

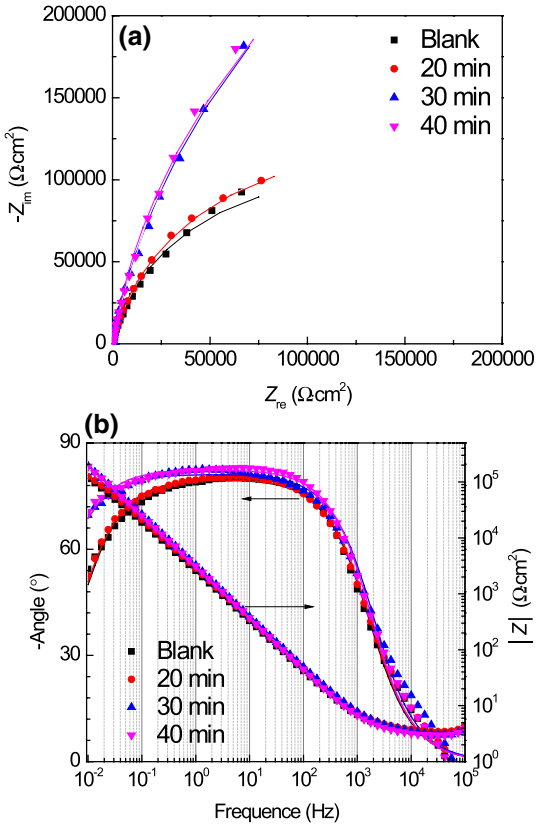

Fig. 2 Electrochemical impedance spectra of passivated 304 SS in 3.5% NaCl solution. (All the 304 SS specimens were passivated in alkaline phosphate solution for different lengths of time; original data are depicted as points, and the corresponding fitting results are shown as lines.) **a** Nyquist plots, **b** Bode plots

Table 2 Fitted electrochemical parameters of passivated 304 SS in 3.5% NaCl solution (All the 304 SS specimens were passivated in alkaline phosphate solution at temperatures of 90 °C, 100 °C, and 110 °C)

Condition (°C)	R_s (Ω cm^2)	Q (Ω^{-1} cm^{-2} s^{-n})	n	R_t (Ω cm^2)
Blank	3.468 (2.211%)	7.774×10^{-5} (1.751%)	0.8874 (0.400%)	2.309×10^5 (9.708%)
90	3.260 (3.321%)	5.809×10^{-5} (2.544%)	0.8951 (0.555%)	2.650×10^5 (12.220%)
100	2.833 (3.100%)	5.728×10^{-5} (2.289%)	0.9012 (0.493%)	3.889×10^5 (14.860%)
110	4.704 (1.549%)	7.626×10^{-5} (1.229%)	0.8922 (0.294%)	1.365×10^6 (35.240%)

Fitting errors are listed in parentheses

Table 3 Fitted electrochemical parameters of passivated 304 SS in 3.5% NaCl solution (304 SS specimens were passivated in phosphate passivation solution at 110 °C for different lengths of time)

Condition (min)	R_s (Ω cm^2)	Q (Ω^{-1} cm^{-2} s^{-n})	n	R_t (Ω cm^2)
Blank	3.468 (2.211%)	7.774×10^{-5} (1.751%)	0.8874 (0.400%)	2.309×10^{5} (9.708%)
20	3.654 (1.750%)	7.008×10^{-5} (1.374%)	0.8883 (0.312%)	2.666×10^{5} (7.896%)
30	4.704 (1.549%)	7.626×10^{-5} (1.229%)	0.8922 (0.294%)	1.365×10^{6} (35.240%)
40	3.195 (2.204%)	5.974×10^{-5} (1.669%)	0.9169 (0.367%)	8.261×10^{5} (21.770%)

Fitting errors are listed in parentheses

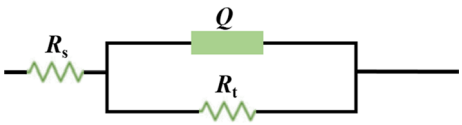

Fig. 3 Electrochemical equivalent circuit used to simulate the EIS data of 304 SS covered by passive film

the Nyquist plots. These results indicate that the formation of passive film in passivation solution A reached a stable state after 30 min. The interface capacitance Q decreased along with the passivation time, which demonstrates that a well-passivated film inhibits the adsorption of Cl^-.

Passivation Behavior in Alkaline Phosphate–Molybdate Solution

To investigate the effect of molybdate on passivation, a 304 SS specimen was immersed in solution B at various temperatures, after which the corrosion resistance was measured in the NaCl solution (Fig. 4). The passivation time for all experiments was 30 min. As shown in Fig. 4a, the capacitance arcs first increase and then decrease as the temperature increases from 40 to 110 °C. The Bode plots shown in Fig. 4b exhibit similar trends. The fitting results shown in Table 4 reveal that R_s first increases and then decreases, and Q shows the reverse trend. The decreased corrosion resistance at 110 °C is possibly because the thick film that formed at high temperature may have had more defects, which degraded the corrosion resistance [36].

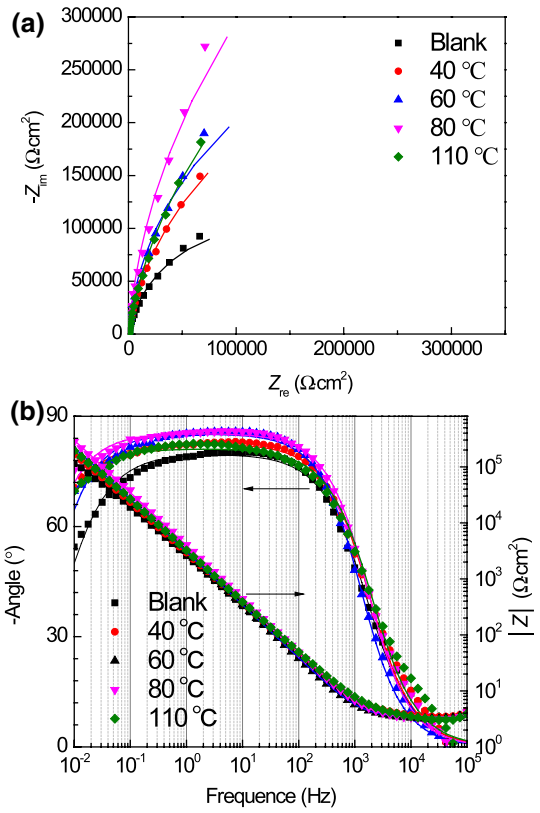

Fig. 4 Electrochemical impedance spectra of passivated 304 SS in 3.5% NaCl solution. (All the 304 SS specimens were passivated in alkaline phosphate–molybdate solution for different lengths of time; original data are depicted as points, and the corresponding fitting results are shown as lines.) **a** Nyquist plots, **b** Bode plots

Surface Morphology and Composition of the Passive Film

The morphology and composition of the passive film were determined using an SEM equipped with EDS, the results of which are shown in Figs. 5 and 6. The untreated 304 SS had a uniform surface with some scratches due to abrading that can be clearly seen. Figure 5b shows the EDS results of the region highlighted by the red box in Fig. 5a. The passive film contains O (2.009%), P (0.088%), S (0.015%), Cr (19.165%), Fe (70.833%), and Ni (7.755%). Figure 5c, d shows the element mapping results for Fe and P, respectively. We can see that P was distributed uniformly on the surface, and that the passive film is an oxide layer successfully modified by P. P may play a major role in enhancing the stability of the passive film.

Figure 6c–e presents the element mapping results of Fe, P, and Mo. After passivation in solution B, the P content increased by a factor of five relative to that of the untreated sample (Fig. 6b). The passive film contains O (0.017%), P (0.478%), S (0.001%), Cr (18.814%), Fe (71.962%), and Ni (8.568%). In addition, Mo (0.161%) is detected on the

Table 4 Fitted electrochemical parameters of passivated 304 SS in 3.5% NaCl solution (304 SS specimens were passivated in phosphate–molybdate solution at different temperatures)

Condition (°C)	R_s (Ω cm^2)	Q (Ω^{-1} cm^{-2} s^{-n})	n	R_t (Ω cm^2)
Blank	3.468 (2.211%)	7.774×10^{-5} (1.751%)	0.8874 (0.400%)	2.309×10^{5} (9.708%)
40	3.661 (1.686%)	6.556×10^{-5} (1.299%)	0.9026 (0.294%)	5.675×10^{5} (13.410%)
60	3.401 (1.970%)	5.759×10^{-5} (1.573%)	0.9480 (0.344%)	6.092×10^{5} (13.770%)
80	3.366 (2.044%)	4.457×10^{-5} (1.561%)	0.9485 (0.332%)	1.268×10^{6} (21.470%)
110	3.336 (2.126%)	5.896×10^{-5} (1.581%)	0.9026 (0.350%)	8.944×10^{5} (22.760%)

Fitting errors are listed in parentheses

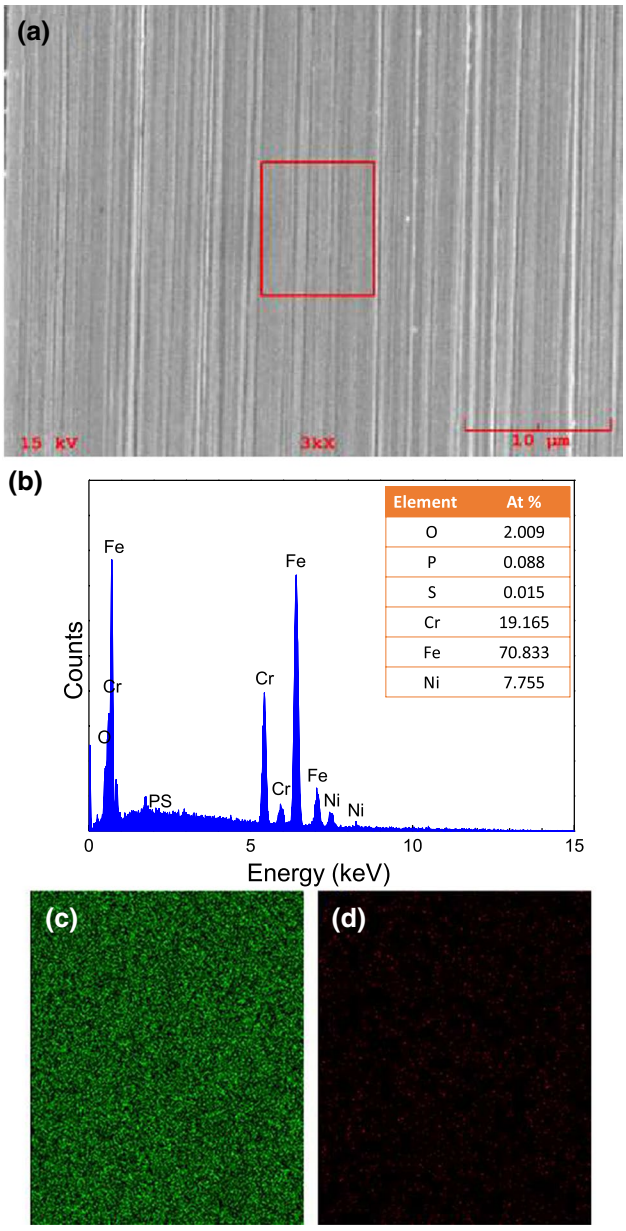

Fig. 5 Surface morphology and energy spectrum of untreated 304 SS. **a** SEM image, **b** EDS analysis, **c** Fe mapping, **d** P mapping

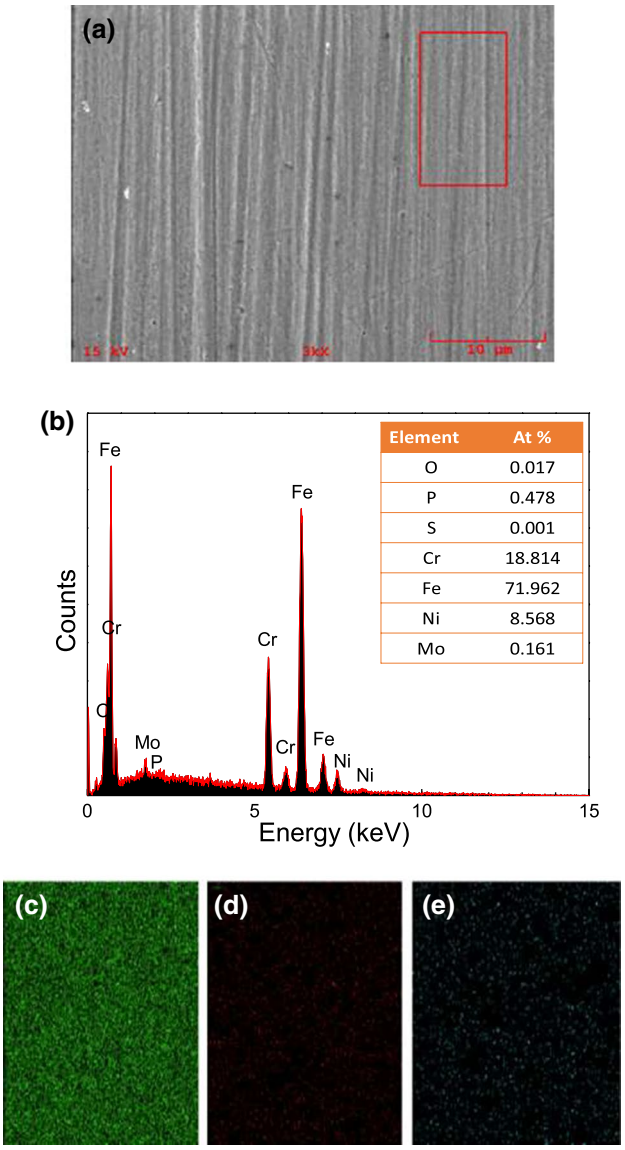

Fig. 6 Surface morphology and energy spectrum of 304 SS passivated at 80 °C for 30 min in alkaline phosphate–molybdate passivation solution. **a** SEM image, **b** EDS analysis, **c** Fe mapping, **d** P mapping, and **e** Mo mapping

surface, which indicates that the passive film is modified by Mo. The effect of Mo on pitting corrosion has been well documented, but the mechanism remains a matter of debate. The role of Mo in enhancing the pitting potential is possibly based on one of the following reasons:

1. Mo-containing alloys resist pitting. This effect is likely provided by Mo^{6+} locally enriched on the film surface [24, 37];
2. Mo slows the dissolution kinetics after the initiation of pitting [38].

Details of this mechanism were not determined or confirmed in this work because the chemical modification of the passive film that forms on 304 SS is at the nano- or atomic level. To clarify these changes at atomic level, advantage characterization techniques and atomic modeling are favorable. In future work, we may use a spherical aberration correction in a transmission electron microscope to observe the structure and composition of the passive film at very high resolution.

Conclusions

1. The corrosion resistance of the passive film was enhanced after passivation in alkaline phosphate solutions, as compared to that of the blank sample. P was detected and found to be uniformly distributed on the film surface, which is beneficial to passivity.
2. The solution temperature and passivation time of the alkaline phosphate solutions were found to have a significant effect on the corrosion resistance of passive film, whereby a higher temperature leads to a high-quality film. The best passivation time was determined to be ~ 30 min.
3. The addition of molybdate to the alkaline phosphate solution further enhanced the corrosion resistance of the passive film, as confirmed by EIS analysis.
4. EDS results indicated the detection of Mo and P in the passive film after passivation in alkaline phosphate–molybdate solutions. These results indicate that Mo is beneficial to the stability of the passive film.

Acknowledgements The work was supported by the National Natural Science Foundation of China (No. 51701140).

References

1. Cheng X, Luo H, Xiao K et al (2017) Investigation on electrochemical corrosion of 304 stainless steel under thin electrolyte layers containing chloride ions. Int J Electrochem Sci 12:8006–8020
2. Xia D, Sun Y, Fan H (2015) Characterization of passive film formed on 304 SS in simulated alkaline water chemistries containing sulfur at 300 °C. Trans Tianjin Univ 21:554–561
3. Hu S, Pang J, Shen J et al (2016) Microstructure, mechanical property and corrosion resistance property of $Cr_{26}Mo_{3.5}$ super ferritic stainless joints by P-TIG and laser welding. Trans Tianjin Univ 22:451–457
4. Luo H, Li XG, Xiao K et al (2013) Corrosion behavior of 304 stainless steel in the marine atmospheric environment of Xisha islands. J Univ Sci Technol Beijing 35:332–338 **(in Chinese)**
5. Zhang B, Wang J, Wu B et al (2018) Unmasking chloride attack on the passive film of metals. Nature Communications. https://doi.org/10.1038/s41467-018-04942-x
6. Macdonald DD, Lei X (2016) Theoretical interpretation of anion size effects in passivity breakdown. J Electrochem Soc 163:C738–C744
7. Frankel GS, Li T, Scully JR (2017) Perspective—Localized corrosion: passive film breakdown vs pit growth stability. J Electrochem Soc 164:C180–C181
8. Li T, Scully J, Frankel G (2018) Localized corrosion: passive film breakdown vs pit growth stability: Part II. A model for critical pitting temperature. J Electrochem Soc 165:C484–C491
9. Xia D-H, Behnamian Y, Luo JL (2019) Factors influencing sulfur induced corrosion on the secondary side in pressurized water reactors (PWRs). J Electrochem Soc 166:C49–C64
10. Natishan P, O'grady W (2014) Chloride ion interactions with oxide-covered aluminum leading to pitting corrosion: a review. J Electrochem Soc 161:C421–C432
11. Wang Y, Song S, Wang J et al (2019) Correlation between passivity breakdown and composition of passive film formed on alloy 690 studied by sputtering XPS and FIB-HRTEM. J Electrochem Soc 166:C332–C344
12. Gao Z, Wang Z, Sun Y et al (2016) Passivity degradation of nuclear materials in reduced sulfur environments: a review. Trans Tianjin Univ 22:189–201
13. Xia D-H, Luo JL (2015) Passivity degradation of alloy 800 in simulated crevice chemistries. Trans Tianjin Univ 21:234–243
14. Fernández J, El Ouardi Y, Bonastre J et al (2019) Modification of the magnesium corrosion rate in physiological saline 0.9 wt% NaCl via chemical and electrochemical coating of reduced graphene oxide. Corros Sci 152:75–81
15. Kumar V, Ghosh P (2019) Performance evaluation of modified black clay as a heterogeneous fenton catalyst on decolorization of azure B dye: kinetic study and cost evaluation. Trans Tianjin Univ 25:527–539
16. Cui C, Du H, Liu H et al (2020) Corrosion behavior of the electroless Ni-P coating on the pore walls of the lotus-type porous copper. Corros Sci 162:108202
17. Sun C, Zeng H, Luo JL (2019) Unraveling the effects of CO_2 and H_2S on the corrosion behavior of electroless Ni-P coating in CO_2/H_2S/Cl– environments at high temperature and high pressure. Corros Sci 148:317–330

18. Saeidpour F, Zandrahimi M, Ebrahimifar H (2019) Effect of ZrO_2 particles on oxidation and electrical behavior of Co coatings electroplated on ferritic stainless steel interconnect. Corros Sci 153:200–212
19. Abdollahi A, Torabi S, Valefi Z et al (2019) Formation mechanism and supersonic flame erosion behavior of SiC and SiC–SiC nano single-layer oxidation protective coatings for carbon materials by reactive melt infiltration (RMI) method. Corros Sci 159:108136
20. Fathi P, Rafieazad M, Duan X et al (2019) On microstructure and corrosion behaviour of $AlSi_{10}Mg$ alloy with low surface roughness fabricated by direct metal laser sintering. Corros Sci 157:126–145
21. Jin W, Wu G, Feng H et al (2015) Improvement of corrosion resistance and biocompatibility of rare-earth WE43 magnesium alloy by neodymium self-ion implantation. Corros Sci 94:142–155
22. Frankel G, Thornton G, Street S et al (2015) Localised corrosion: general discussion. Faraday Discuss 180:381–414
23. Maurice V, Marcus P (2018) Progress in corrosion science at atomic and nanometric scales. Prog Mater Sci 95:132–171
24. Elbiache A, Marcus P (1992) The role of molybdenum in the dissolution and the passivation of stainless steels with adsorbed sulphur. Corros Sci 33:261–269
25. Akulich N, Ivanova N, Zharskii I et al (2018) Properties of zinc coatings electrochemically passivated in sodium molybdate. Surf Interface Anal 50:1310–1318
26. Tavassolian R, Moayed MH, Taji I (2019) Mechanistic investigation on the effect of molybdate on the critical pitting temperature of 2205 duplex stainless steel. J Electrochem Soc 166:C101–C107
27. Tang PT, Bech-Nielsen G, Møller P (1994) Molybdate based alternatives to chromating as a passivation treatment for zinc. Plat Surf Finish 81:20–23
28. Tsai CY, Liu JS, Chen PL et al (2010) A two-step roll coating phosphate/molybdate passivation treatment for hot-dip galvanized steel sheet. Corros Sci 52:3385–3393
29. Ishizaki T, Masuda Y, Teshima K (2013) Composite film formed on magnesium alloy AZ31 by chemical conversion from molybdate/phosphate/fluorinate aqueous solution toward corrosion protection. Surf Coat Technol 217:76–83
30. Wu S, Wang J, Song S et al (2017) Factors influencing passivity breakdown on UNS N08800 in neutral chloride and thiosulfate solutions. J Electrochem Soc 164:C94–C103
31. Mohammadi M, Choudhary L, Gadala IM et al (2016) Electrochemical and passive layer characterizations of 304L, 316L, and duplex 2205 stainless steels in thiosulfate gold leaching solutions. J Electrochem Soc 163:C883–C894
32. Hien P, Vu N, Thu V et al (2017) Study of yttrium 4-nitrocinnamate to promote surface interactions with AS1020 steel. Appl Surf Sci 412:464–474
33. Nam N, Kim J, Lee Y et al (2009) Effect of thermal treatment on the corrosion resistance of polyaniline in H_2SO_4–HF acid mixture solution. Corros Sci 51:3007–3013
34. Nahali H, Dhouibi L, Idrissi H (2015) Effect of Na_3PO_4 addition in mortar on steel reinforcement corrosion behavior in 3% NaCl solution. Constr Build Mater 78:92–101
35. Xia D-H, Behnamian Y, Feng HN et al (2014) Semiconductivity conversion of Alloy 800 in sulphate, thiosulphate, and chloride solutions. Corros Sci 87:265–277
36. Xia D-H, Sun YF, Shen C et al (2015) A mechanistic study on sulfur-induced passivity degradation on Alloy 800 in simulated alkaline crevice chemistries at temperatures ranging from 21 °C to 300 °C. Corros Sci 100:504–516
37. Newman R (1985) The dissolution and passivation kinetics of stainless alloys containing molybdenum—II. Dissolution kinetics in artificial pits. Corros Sci 25:341–350
38. Marcus P, Olefjord I (1988) A Round Robin on combined electrochemical and AES/ESCA characterization of the passive films on Fe–Cr and Fe–Cr–Mo alloys. Corros Sci 28:589–602

Dr. Da-Hai Xia is a teacher at the School of Materials Science and Engineering, Tianjin University. He joined the postdoctoral fellow (2013–2014) at University of Alberta (Canada) under the guidance of Prof. Jing-Li Luo. His research interests are interdisciplinary studies of corrosion, electrochemistry and surface science.